An antimicrobial helix A-derived peptide of heparin cofactor II blocks endotoxin responses *in vivo*

Praveen Papareddy[1], Martina Kalle[1], Shalini Singh[2], Matthias Mörgelin[3], Artur Schmidtchen[1,4], and Martin Malmsten[2,*]

[1]Division of Dermatology and Venereology, Department of Clinical Sciences, Lund University, SE-221 84 Lund, Sweden

[2]Department of Pharmacy, Uppsala University, SE-75123, Uppsala, Sweden

[3]Division of Infection Medicine, Department of Clinical Sciences, Lund University, SE-221 84 Lund, Sweden

[4]Lee Kong Chian School of Medicine, Nanyang Technological University, 11 Mandalay Road, Singapore 308232

[*]Corresponding author. Tel: +46184714334; Fax: +46184714377; E-mail: martin.malmsten@farmaci.uu.se

Key words: antimicrobial peptide, lipopolysaccharide, lipid A, membrane

Abstract

Host defense peptides are key components of the innate immune system, providing multi-facetted responses to invading pathogens. Here, we describe that the peptide GKS26 (GKSRIQRLNILNAKFAFNLYRVLKDQ), corresponding to the A domain of heparin cofactor II (HCII), ameliorates experimental septic shock. The peptide displays antimicrobial effects through direct membrane disruption, also at physiological salt concentration and in the presence of plasma and serum. Biophysical investigations of model lipid membranes showed the antimicrobial action of GKS26 to be mirrored by peptide incorporation into, and disordering of, bacterial lipid membranes. GKS26 furthermore binds extensively to bacterial lipopolysaccharide (LPS), as well as its endotoxic lipid A moiety, and displays potent anti-inflammatory effects, both *in vitro* and *in vivo*. Thus, for mice challenged with ip injection of LPS, GKS26 suppresses pro-inflammatory cytokines, reduces vascular leakage and infiltration in lung tissue, and normalizes coagulation. Together, these findings suggest that GKS26 may be of interest for further investigations as therapeutic against severe infections and septic shock.

Introduction

Antimicrobial and host defense peptides play a central role in the protection against invading pathogens, providing antimicrobial, anti-inflammatory, as well as other effects (1,2). With increasing resistance development against conventional antibiotics, as well as remaining challenges in the treatment of both acute and chronic inflammation, such peptides have been subject of considerable research interest during the last decade. As part of this, various approaches have been employed for identification of potent, but simultaneously selective, peptides, including, e.g., quantitative structure-activity approaches (3). Within context, we have focused our efforts primarily on peptides derived from endogenous proteins, including complement, coagulation, and matrix proteins, displaying potent antimicrobial effects but also low toxicity to human cells. In addition to such directly antimicrobial effects, some of these studies have also been demonstrated to display potent anti-inflammatory capacity, able to counteract the multiple detrimental effects of bacterial lipopolysaccharide (LPS) from Gram-negative bacteria, as well as related effects from lipoteichoic acid (LTA) from Gram-positive bacteria and zymosan from fungi (4,5).

In our work with coagulation-based host defense peptides and holoproteins, we previously investigated the serine proteinase inhibitor heparin cofactor II (HCII), and were able to demonstrate a novel host defense function of this protein (6). Thus, compared to normal mice, $HCII^{-/-}$ knock-outs were found to be more susceptible to LPS-induced shock and invasive infection by *Pseudomonas aeruginosa*. Concomitantly, a significantly increased cytokine response was observed in $HCII^{-/-}$ mice in response to infection, and HCII levels were reduced in infected normal mice. The LPS-binding, as well as antimicrobial capacity, of activated HCII was furthermore found to be dependent on a conformational change, exposing the amphiphilic and positively charged A and D helices of HCII.

Having shown that these helices are important for the host defense function of HCII, we hypothesized that the epitopes alone could potentially maintain some functional properties of the holoprotein, thus offering interesting opportunities as simpler therapeutic agents. We here describe biological activities of a helix A-derived peptide of HCII, GKS26 (GKSRIQRLNILNAKFAFNLYRVLKDQ), spanning the entire length of the helix. In doing so, we report on its antimicrobial and anti-inflammatory properties, using a battery of assays for broad effect characterization. In parallel, biophysical investigations provided additional insight into the mechanisms underlying these effects. The peptide exerted potent antibacterial and anti-inflammatory activities, and showed efficiency in a model of endotoxin-induced shock *in vivo*. Taken together, the results thus demonstrate this peptide to be of potential interest in the development of novel anti-infective and anti-inflammatory therapies.

Experimental

Chemicals. GKS26 (Table 1) was synthesized by Biopeptide Co., San Diego, USA, and was of >95% purity, as evidenced by mass spectral analysis (MALDI-TOF Voyager). LPS and lipid A from *E. coli* (0111:B4 and F583 (Rd mutant), respectively) were from Sigma (St. Louis, USA). In LPS (>500000 EU/mg), protein and RNA content were both less than 1%.

Microorganisms. *Escherichia coli* (*E. coli*) ATCC 25922, *Pseudomonas aeruginosa* (*P. aeruginosa*) ATCC 27853, *Staphylococcus aureus* (*S. aureus*) ATCC 29213, and *Bacillus subtilis* (*B. subtilis*) ATCC 6633 isolates were obtained from the Department of Clinical Bacteriology at Lund University Hospital, Sweden.

Scanning electron microscopy. Bacteria were grown in TH medium at 37ºC to mid-logarithmic phase. The bacteria were washed in buffer (10 mM Tris, pH 7.4, 0.15 M NaCl, 5 mM glucose) and resuspended in the same buffer. Peptides at 30 μM were incubated with *S. aureus* ATCC 29213 or *P. aeruginosa* ATCC 27853 (1×10^8 bacteria) for two hours in a total volume of 50 ml in 10 mM Tris, pH 7.4, with additional 150 mM NaCl. Bacteria were fixed and prepared for scanning electron microscopy as described previously (7). Samples were examined with a Philips/FEI CM 100 electron microscope operated at 80 kV accelerating voltage and images recorded with a side-mounted Olympus Veleta camera at the Core Facility for integrated Microscopy (CFIM), Copenhagen University, Denmark.

Fluorescence microscopy. For monitoring of membrane permeabilization using the impermeant probe FITC (Sigma-Aldrich, St. Louis, USA), *E. coli* ATCC 25922 bacteria were grown to mid-logarithmic phase in TSB medium. Bacteria were washed and re-suspended in buffer (10 mM Tris, pH 7.4, 0.15M NaCl) to yield a suspension of $1x10^7$ CFU/ml. 100 ml of the bacterial suspension was incubated with 30 μM of the respective peptides at 37°C for 60 min. Microorganisms were then immobilized on poly (L-lysine)–coated glass slides by incubation for 45 min at 30°C, followed by addition onto the slides of 200 ml of FITC (6 mg/ml) in buffer and incubation for 30 min at 30°C. The slides were washed and bacteria fixed by incubation, first on ice for 15 min, then in room temperature for 45 min in 4% paraformaldehyde. The glass slides were subsequently mounted on slides using Prolong Gold anti-fade reagent mounting medium (Invitrogen, Eugene, USA). For fluorescence analysis, bacteria were visualized using a Nikon Eclipse TE300 (Nikon, Melville, USA) inverted fluorescence microscope equipped with a Hamamatsu C4742-95 cooled CCD camera (Hamamatsu, Bridgewater, USA) and a Plan Apochromat ×100

objective (Olympus, Orangeburg, USA). Differential interference contrast (Nomarski) imaging was used for visualization of the microbes themselves.

Liposome preparation and leakage assay. Model liposomes investigated were anionic (DOPE/DOPG 75/25 mol/mol), frequently used as bacteria membrane models (8). DOPG (1,2-dioleoyl-*sn*-Glycero-3-phosphoglycerol, monosodium salt) and DOPE (1,2-dioleoyl-*sn*-Glycero-3-phosphoethanolamine) were from Avanti Polar Lipids (Alabaster, USA) and of >99% purity. In addition, reconstituted lipid membranes were used based on polar extract of *E. coli*, with a lipid composition of 67.0% phosphatidylethanolamine, 23.2% phosphatidylglycerol, and 9.8% diphosphatidylglycerol (Avanti Polar Lipids; Alabaster, USA). The lipid mixture was dissolved in chloroform, after which solvent was removed by evaporation under vacuum overnight. Subsequently, 10 mM Tris buffer, pH 7.4, was added together with 0.1 M carboxyfluorescein (CF) (Sigma, St. Louis, USA). After hydration, the lipid mixture was subjected to eight freeze-thaw cycles (not for *E. coli* liposomes), consisting of freezing in liquid nitrogen and heating to 60°C. Unilamellar liposomes of about Ø140 nm were generated by multiple extrusions (30 passages) through polycarbonate filters (pore size 100 nm) mounted in a LipoFast miniextruder (Avestin, Ottawa, Canada) at 22°C. Untrapped CF was removed by two subsequent gel filtrations (Sephadex G-50, GE Healthcare, Uppsala, Sweden) at 22°C, with Tris buffer as eluent. CF release from the liposomes was determined by monitoring the emitted fluorescence at 520 nm from a liposome dispersion (10 μM lipid in 10 mM Tris, pH 7.4). For the leakage experiment in the presence of LPS, 0.02 mg/ml LPS was first added to the above liposome dispersion (which did not cause liposome leakage in itself; results not shown), after which peptide was added and leakage monitored as a function of time. An absolute leakage scale was obtained by disrupting the liposomes at the end of each experiment through addition of 0.8 mM Triton X-100 (Sigma-Aldrich, St. Louis, USA).

A SPEX-fluorolog 1650 0.22-m double spectrometer (SPEX Industries, Edison, USA) was used for the liposome leakage assay. Measurements were performed in triplicate at 37 °C.

CD spectroscopy. Circular dichroism (CD) spectra were measured by a Jasco J-810 Spectropolarimeter (Jasco, Easton, USA). Measurements were performed in duplicate at 37°C in a 10 mm quartz cuvette under stirring with a peptide concentration of 10 μM. The effect on peptide secondary structure of liposomes at a lipid concentration of 100 μM was monitored in the range 200-260 nm. The α-helix content was calculated from the recorded CD signal at 225 nm using reference peptides in purely helical and random coil conformations, respectively. 100% α-helix and 100% random coil references were obtained from 0.133 mM (monomer concentration) poly-L-lysine (M_w = 79 kDa) in 0.1 M NaOH and 0.1 M HCl, respectively. For measurements in the presence of LPS, 0.2 mg/ml was used. To account for instrumental differences between measurements, background subtraction was performed routinely. Signals from the bulk solution were also corrected for.

Ellipsometry. Peptide adsorption to supported lipid bilayers was studied *in situ* by null ellipsometry, using an Optrel Multiskop (Optrel, Kleinmachnow, Germany) equipped with a 100 mW Nd:YAG laser (JDS Uniphase, Milpitas, USA). All measurements were carried out at 532 nm and an angle of incidence of 67.66° in a 5 ml cuvette under stirring (300 rpm). Both the principles of null ellipsometry and the procedures used have been described extensively before (9). In brief, measurements were first made on the bare silica surface, which allows its complex refractive index to be determined. These parameters were subsequently used together with new sets of the optical component positions after adsorbed layer formation for determining the thickness and refractive index of the adsorbed layer. From this, the mean

refractive index (n) and layer thickness (d) of the adsorbed layer can be obtained. From the thickness and refractive index the adsorbed amount (Γ) was calculated according to:

$$\Gamma = \frac{(n - n_0)}{dn/dc} d \qquad (1)$$

where n_0 is the refractive index of the bulk solution, and dn/dc the refractive index increment (0.154 cm^3/g). Corrections were routinely done for changes in bulk refractive index caused by changes in temperature and excess electrolyte concentration.

LPS-coated surfaces were obtained by adsorbing *E. coli* LPS to methylated silica surfaces (surface potential -40 mV, contact angle 90° (10)) from 5 mg/ml LPS stock solution in water at a concentration of 0.4 mg/ml over a period of 2 hours. This results in a hydrophobically driven LPS adsorption of 1.48±0.38 mg/m^2, corresponding to plateau in the LPS adsorption isotherm under these conditions. Non-adsorbed LPS was removed by rinsing with Tris buffer at 5 ml/min for a period of 30 minutes, followed by buffer stabilization for 20 minutes. Peptide addition was performed at different concentrations of 0.01, 0.1, 0.5, and 1 μM, and the adsorption monitored for one hour after each addition. All measurements were performed in at least duplicate at 25°C. For lipid A deposition, this was solubilized with 0.25 wt % triethyl amine (TEA) under vigorous vortexing and heating to 60 ^{0}C for 10 minutes. Lipid A was adsorbed at methylated silica surfaces for 2 hours from 5 mg/ml lipid A stock solution in 0.25 % TEA at a concentration of 0.4 mg/ml in 10 mM Tris, pH 7.4, containing 150 mM NaCl. Non-adsorbed lipid A was subsequently removed by rinsing with same buffer at 5 ml/min for 15 minutes, followed by buffer stabilization for 20 minutes. This results in a lipid A adsorption of 0.8±0.2 mg/m^2. Peptide addition was subsequently performed to 0.01, 0.1,

0.5, and 1 μM, and adsorption monitored for one hour after each addition. All measurements were performed in at least duplicate at 25°C.

Supported lipid bilayers were generated by liposome adsorption. DOPE/DOPG (75/25 mol/mol) liposomes were prepared as described above, but the dried lipid films resuspended in Tris buffer only with no CF present. In order to avoid adsorption of peptide directly at the silica substrate through any defects of the supported lipid layer, poly-L-lysine (M_w = 170 kDa, Sigma-Aldrich, St. Louis, USA) was preadsorbed from water prior to lipid addition to an amount of 0.045 ± 0.01 mg/m^2, followed by removal of nonadsorbed poly-L-lysine by rinsing with water at 5 ml/min for 20 minutes (11). Water in the cuvette was then replaced by buffer containing also 150 mM NaCl, followed by addition of liposomes in buffer at a lipid concentration of 20 μM, and subsequently by rinsing with buffer (5 ml/min for 15 minutes) when liposome adsorption had stabilised. The final layer formed had structural characteristics (thickness 4±1 nm, mean refractive index 1.47±0.03), suggesting that a layer fairly close to a complete bilayer is formed. After lipid bilayer formation, the cuvette content was replaced by 10 mM Tris buffer at a rate of 5 ml/min over a period of 30 minutes. After stabilization for 40 minutes, peptide was added to a concentration of 0.01 μM, followed by three subsequent peptide additions to 0.1 μM, 0.5 μM, and 1 μM, in all cases monitoring the adsorption for one hour. All measurements were made in at least duplicate at 25°C.

Dual polarization interferometry. Peptide disordering of DOPE/DOPG supported bilayers were investigated by dual polarization interferometry (DPI), using a Farfield AnaLight 4D (Biolin Farfield, Manchester, U.K.), operating with an alternating 632.8 nm laser beam. The technique is based on a dual slab waveguide, consisiting of an upper sensing waveguide (supporting the lipid bilayer) and a lower reference waveguide. The changes induced by the

peptide/lipid adsorption was monitored through changes in the transverse electric and transverse magnetic modes as described previously (12). As for ellipsometry, Eq. 1 was used for determining the mass adsorbed. Although treating phospholipids as optically isotropic systems is a reasonably accurate approximation for unsaturated and disorganized phospholipid bilayers, these actually display some optical birefringence, which is measurable with the sensitive DPI technique. DPI allows two parameters to be obtained from each measurement, e.g., for the simultaneous determination of two optical parameters of the adsorbed layer. The latter were chosen to be the adsorbed amount and the anisotropy, assuming the adsorbed layer thickness to be constant during the adsorption process. The birefringence (Δn_f), obtained from the refractive indices for the TM and TE waveguide modes, reflects ordering of the lipid molecules in the bilayer, and decreases with increasing disordering of the bilayer (13). Consequently, Δn_f can be used to monitor disordering transitions in lipid bilayers, e.g., as a result of peptide binding and incorporation, and therefore offers a simpler alternative to, e.g., order parameter analyses in ^{2}H-NMR spectroscopy (14). In the present study, DOPE/DOPG liposomes (75/25 mol/mol) were prepared as described above for ellipsometry, and the liposomes (at a lipid concentration of 0.2 mg/ml in 10 mM HEPES buffer, containing also 150 mM NaCl and 1.5 mM $CaCl_2$) fused to the silicon oxynitride/silicon substrate (contact angle <5°) at a flow rate of 25 μL/min for 8 minutes. This resulted in bilayer formation, characterized by a refractive index of 1.47, a thickness of 4.5±0.3 nm, and an area per molecule of 54 Å^2. After bilayer formation, the buffer was changed to 10 mM Tris buffer, allowing continous flushing (at flow rate, 50 μl/ min) for 10 minutes, after which peptide was added at the desired concentration. Peptide adsorption was monitored for one hour. Measurements were performed at least in duplicate at 25°C.

Radial diffusion assay. Essentially as described before (15,16), bacteria were grown to mid-logarithmic phase in 10 ml of full-strength (3% w/v) trypticase soy broth (TSB) (Becton-Dickinson, Cockeysville, USA) (enzymatic digest of casein (17 g/L) and soybean (3 g/L), glucose (2.5 g/L), sodium chloride (5 g/L), and dipotassium hydrogen phosphate (2.5 g/L), pH 7.3). The microorganisms were then washed once with 10 mM Tris, pH 7.4. Subsequently, 4 x 10^6 bacterial colony forming units (cfu) were added to 15 ml of the underlay agarose gel, consisting of 0.03% (w/v) TSB, 1% (w/v) low electroendosmosis type (EEO) agarose (Sigma-Aldrich, St Louis, USA), and 0.02% (v/v) Tween 20 (Sigma-Aldrich, St Louis, USA), with or without 150 mM NaCl. The underlay was poured into a Ø 144 mm petri dish. After agarose solidification, 4 mm-diameter wells were punched and 6 µl of test sample added to each well. Plates were incubated at 37ºC for 3 hours to allow diffusion of the peptides. The underlay gel was then covered with 15 ml of molten overlay (6% TSB and 1% Low-EEO agarose in distilled H_2O). Antimicrobial activity of a peptide is visualized as a zone of clearing around each well after 18-24 hours of incubation at 37°C.

Viable-count analysis. Bacteria were grown to mid-logarithmic phase in Todd-Hewitt (TH) medium (heart infusion (3.1 g/L), yeast-enriched peptone (20 g/L), glucose (2 g/L), sodium chloride (2 g/L), disodium phosphate (0.4 g/L), and sodium carbonate (2.5 g/l), pH 7.8), and then washed and diluted in 10 mM Tris, pH 7.4, 5 mM glucose, 0.15 M NaCl. Following this, bacteria (50 µl of 2 x 10^6 cfu/ml) were incubated at 37°C for 2 hours in the presence of peptide at indicated concentrations in 10 mM Tris, 0.15 M NaCl, with or without 20% human citrate-plasma (CP) or 20% serum. Serial dilutions of the incubation mixture were plated on TH agar, followed by incubation at 37°C overnight and cfu determination.

LPS effects on macrophages *in vitro.* RAW 276.4 cells (3.5×10^6 cells/ml) (ATCC TIB 71, American Type Culture Collection, Manassas, USA) were seeded in 96-well tissue culture plates (Nunc) in phenol red-free Dulbecco´s modified Eagle medium (DMEM; PAA laboratories) supplemented with 10% (v/v) heat-inactivated fetal bovine serum (FBS); Invitrogen) and 1% (v/v) Antibiotic-Antimycotic solution (ASS; Invitrogen). After 20 h of incubation to permit adherence, cells were stimulated with 10 ng/mL *E. coli* LPS (0111:B4) (Sigma-Aldrich), and various doses of GKS26. The level of nitrite oxide (NO) in culture supernatants was determined after 20 h incubation at 37°C and 5% CO_2 using the Griess reaction as described previously (17). In addition, RAW-Blue™ cells ($1x10^6$ cells/ml) (InvivoGen) were seeded in phenol red-free DMEM, supplemented with 10% (v/v) heat-inactivated FBS and 1% (v/v) AAS, and allowed to adhere before they were stimulated with 10 - 1000 ng/ml *E. coli* (0111:B4) LPS and 10 µM GKS26. NF-κB activation was determined after 20 h of incubation according to manufacturers instructions (InvivoGen). Briefly, activation of NF-κB leads to the secretion of embryonic alkaline phosphatase (SEAP) into the cell supernatant were it was measured by mixing supernatants with a SEAP detection reagent (Quanti-Blue™, InvivoGen) followed by measurement of the absorbance (A) at 600 nm.

Lactate dehydrogenase assay. RAW-Blue™ cells ($5\text{-}6\times10^6$ cells/ml) were stimulated as described for the NF-κB activation assay. Lactate dehydrogenase (LDH) release was quantified using the TOX-7 kit (Sigma-Aldrich). After incubation overnight, 50 µl of cell supernatant was mixed with 100 µl LDH reagent mixture, incubated for 5-10 min at RT in the dark before absorption was measured at 490 nm. The percentage of LDH release was calculated as follows: $((A_{490}$ sample - A_{490} negative control)*100)/(A_{490} positive control - A_{490} negative control). The positive control consistent of cells lysed with LDH lysis buffer for 45 min, at 37° C considered as 100 % LDH release.

Whole blood assay. Human lepirudin blood from healthy volunteers was diluted in PBS (1:4 v/v) before the addition of 100 ng/ml *E. coli* (0111:B4) LPS and 10 μM GKS26. After incubation at 37°C overnight, 5 % CO_2 in cell culture plates (Nunc), samples were centrifuged and supernatants were collected and stored at -20°C prior to cytokine analysis.

LPS animal model. All animal experiments were approved by the Laboratory Animal Ethics Committee of Malmö/Lund, Sweden. The animals were obtained from the animal facility at the University of Lund, and housed under standard conditions of light and temperature with free access to laboratory chow and water. Male C57BL/6 mice (8 weeks) were injected intraperitoneally (ip) with 18 mg/kg *E. coli* 0111:B4 LPS (Sigma-Aldrich, ≈500.000 endotoxin units/mg). Thirty minutes after LPS injection, 200 or 500 μg GKS26 in 10 mM Tris, pH 7.4, or buffer alone (control), were injected ip into the mice. The mice were sacrificed after 20 h to determine platelet counts, cytokines, and coagulation parameter. The number of platelets was determined using the VetScan HM5 System (TRIOLAB, Mölndal, Sweden).

Histochemistry. Organs were collected 20 h after LPS injection and immediately fixed in 4% formaldehyde (Histolab AB, Göteborg, Sweden) prior to paraffin embedding and sectioning. Sections were stained with Mayers Haematoxylin (Histolab AB, Göteborg, Sweden) and Eosin (Merck).

Cytokine assay. The levels of IL-6, IL-10, MCP-1, INF-γ, and TNF-α were assessed using the Mouse Inflammation Kit (Becton Dickinson AB, Stockholm, Sweden), according to the manufacturer's instructions. The levels of IL-6, TNF-α, and IL-10 were measured in

supernatants of whole blood using CytoSets™ (Invitrogen) according to manufacture´s instructions.

Coagulation assays. Clotting times were analyzed using an Amelung coagulometer (Lemgo, Germany). Activated partial thromboplastin time (aPTT) was measured by incubating 50 µl citrated mouse plasma for 1 min followed by the addition of 50 µl Dapttin (Technoclone, Vienna Austria) for 200 seconds at 37°C. Clotting was initiated by the addition of 50 µl of $CaCl_2$ (30 mM). For the prothrombin time (PT), clotting was initiated by addition of 50 µl TriniClot-PT Excel (Trinity Biotech, Wicklow, Ireland) to 50 µl of pre-warmed mouse citrate plasma.

Results

GKS26 is antimicrobial *in vitro* and *ex vivo*. First, radial diffusion (RDA) and viable count (VCA) assays were performed to probe direct bactericidal effects of GKS26. As shown in Figure 1A and B, GKS26 displays potent antimicrobial effects against Gram-negative *E. coli* and *P. aeruginosa*, as well as Gram-positive *S. aureus* and *B. subtilis*. Furthermore, Figure 1C demonstrates similar kinetics of this effect for *E. coli* and *P. aeruginosa*. While some of the antimicrobial activity is lost in the presence of serum, high antimicrobial activity is observed in the presence of CP (Figure 1B). The latter is noteworthy, since binding of cationic AMPs to net negatively charged serum proteins frequently results in considerable loss in antimicrobial effects (8). The finding that plasma even accentuates the antimicrobial effects demonstrates that fibrinogen and other coagulation factors may in fact contribute to bactericidal effects, presumably through membrane interactions of highly surface active fibrinogen (18,19). Adding to this, Figure 2 shows GKS26 to display pronounced selectivity between bacteria and mammalian cells. Thus, for *P. aeruginosa* and *E. coli* added to human blood, the peptide is

able to potently kill bacteria, but at the same time not cause hemolysis much above that of the negative control. For *S. aureus*, this selectivity in blood is less pronounced.

GKS26 interacts with bacterial lipid membranes. As demonstrated by peptide-induced release of intracellular material, as well as by FITC permeation, the antimicrobial effect of GKS26 is caused by bacterial membrane lysis (Figure 3A and B). Analogously, GKS26 causes lysis of liposomes composed of model anionic phospholipids (DOPE/DOPG), as well as liposomes composed of *E. coli* lipid extract (Figure 4). As seen, the DOPE/DOPG model liposomes behaved similarly to liposomes formed by *E. coli* lipid extract, demonstrating the experimentally preferred DOPE/DOPG to be a good model for *E. coli* lipid membranes. Taken together, the combined bacteria and liposome data clearly show bacterial membrane disruption to play a key role in the antimicrobial action of GKS26.

The mechanism of lipid membrane disruption was next investigated by studies of peptide binding, insertion, and disordering to/of supported lipid membranes. As shown in Figure 5A, GKS26 displays concentration-dependent adsorption at the anionic DOPE/DOPG lipid membrane, reaching high adsorption densities at concentration corresponding to maximum membrane lysis. Thus, an adsorption density of ≈450 nmol/m^2 corresponds to one peptide molecule per 8 lipid molecules. As shown in Figure 5B, peptide binding to supported DOPE/DOPG lipid bilayers results in a monotonous decrease in the membrane optical anisotropy, indicating that peptide adsorption results in disordering of the lipid membrane. Importantly, there is no threshold for membrane insertion. Instead, the DPI results clearly reports on a continuous process, where all peptides bound to the membrane are inserted into the membrane (as opposed to sitting on-top), throughout the binding process, undergoing modest conformational changes in the process (Figure 5C).

GKS26 interacts with bacterial lipopolysaccharide and reduces LPS responses *in vitro, ex vivo,* and *in vivo*. Moreover, GKS26 displays extensive binding to both *E. coli* LPS and its endotoxic lipid A moiety (Figure 6A), causing a pronounced structure transition in the LPS/peptide complex (Figure 6B). As shown in Figure 4, GKS26 binds preferentially to LPS over the lipid membrane. In previous reports it has been shown that binding to LPS, especially the lipid A moiety, is a prerequisite for anti-inflammatory effects of amphiphilic peptides (20). Therefore, experiments were performed to investigate whether this is the case also for GKS26. Studies using mouse macrophages revealed that GKS26 dose-dependently reduced the LPS-induced production of nitric oxide (Figure 7A). After recognition of LPS via the TLR4-MD2 complex, a signaling cascade is initiated leading to the activation of NF-κB and finally to cytokine production and release (21-23). In experiments using a NF-κB reporter cell line (RAW Blue cells), the data show that GKS26 significantly reduces NF-κB activation (Figure 7B). Moreover the data reveal that this inhibition depends on the ratio of LPS and peptide, indicating that direct LPS scavenging is indeed important for this effect by GKS26. This is further supported by data from a LDH assay, showing no toxic effects of the peptide on RAW-Blue cells (Figure 7C), thus the reduction is at least partly due to LPS-GKS26 interactions and not due to toxicity. Moreover these LDH data are consistent with reduced toxicity seen in blood (Figure 2B). Finally, effects of GKS26 on LPS-induced cytokine release were determined *ex vivo* using a whole blood model. The data show that GKS26 reduced the pro-inflammatory cytokines TNF-α and IL-6, but had no effect on anti-inflammatory IL-10 release (Figure 7D).

Having demonstrated potential anti-inflammatory effects of GKS26 *in vitro*, but also *ex vivo*, a next set of experiments was performed to investigate those in an *in vivo* context. C57BL/6

mice were challenged with 18 mg/kg *E. coli* LPS and treated with either 200 μg of 500 μg of GKS26. Consistent with the data of the whole blood experiments, GKS26 treatment resulted in a dose-dependent reduction of the pro-inflammatory cytokines IL-6, TNF-α, MCP-1, and IFN-γ, as well as in IL-10 (Figure 7E). In parallel, peptide treatment improved the overall status of these animals as illustrated by improved health scoring (Figure 7F).

Inflammation is an important initiator of coagulation (24). Furthermore, systemic activation of coagulation is a compromising factor in sepsis, characterized by consumption of coagulation factors and excessive fibrinolysis, leading to e.g. prolonged coagulation times and thrombocytopenia in patients (25). Compatible to these symptoms are results on platelet levels, as well as clotting times in mice challenged with LPS (Figure 7G and H). The latter displayed prolonged clotting times and a significant reduction in platelets, in contrast to mice treated with GKS26, which showed normalization of both the activated partial thromboplastin time (aPTT) and the prothrombin time (PT) (Figure 7G), as well less partial recovery of platelet numbers (Figure 7H). Examination of mouse lungs further revealed a reduction of disease symptoms, as illustrated by reduced vascular leakage, infiltration of inflammatory and red blood cells, and less reduction in alveolar space for peptide-treated animals compared to LPS-treated ones (Figure 7I), effects particularly clear at the higher concentration of GKS26. Taken together, these findings demonstrate that treatment with GKS26 dampened a range of sepsis-associated pathologies, including the release of pro-inflammatory cytokines, vascular leakage, excessive coagulation, as well as platelet consumption.

Discussion

With its high net charge and intermediate hydrophobicity (Table 1), GKS26 is highly amphiphilic, thus binding readily to lipid membranes. As demonstrated by the DPI

experiments, peptide binding is accompanied by peptide insertion into the membrane throughout the binding process, without a threshold density prior to insertion. While the interplay between peptide binding and insertion is relatively sparsely investigated in literature, these findings are in line with results found for aurein 1.2 on *E. coli* extract and DMPE/DMPG bilayers (26), HCII-derived KYE28 (27), as well as peptides derived from S1 peptidases at DOPE/DOPG bilayers (28). As a result of peptide insertion into the lipid membrane, the latter is destabilized, illustrated by peptide-induced liposome leakage. Importantly, there is a clear correlation between peptide binding density/insertion, destabilization of both model DOPE/DOPG liposomes and liposomes composed of *E. coli* lipid extract, and bacteria lysis, the latter in turn causing bactericidal effects. Importantly, however, GKS26 displays selectivity between bacteria and human cells, demonstrated by the combined bactericidal and hemolysis assays on blood supplemented with bacteria. Such selectivity has previously been observed, e.g., for highly charged and simultaneously moderately hydrophobic peptides (29), and is due to lower peptide binding caused by the lower charge density of the human cell membranes, combined with resistance to peptide insertion caused by the presence of cholesterol.

LPS is a negatively charged lipopolysaccharide, anchored to the outer membrane in Gram-negative bacteria through its hydrophobic lipid A moiety (20). Through complex formation with lipopolysaccharide-binding protein (LBP) by its lipid A moiety, and subsequent recognition of CD14 and the Toll-like receptor 4 (TLR4), LPS causes an up-regulation of pro-inflammatory cytokine production (21-23). Consequently, peptides can provide anti-endotoxic through direct binding to lipid A, precluding or inhibiting LBP binding. It has also been found, however, that LPS aggregates are particularly potent in their endotoxic effect (30), presumably through providing an alternate cell uptake route to the LBP/CD14 receptor one.

Thus, peptides can reach anti-endotoxic effects also through causing disruption of LPS aggregates (27,31,32). Mirroring this, it was recently demonstrated that peptide-induced LPS disaggregation is correlated to pronounced structure transition in the LPS/peptide complex (27,28), as presently observed for GKS26.

Due to its central role for the understanding of peptides of the innate immune system, as well as the need for novel anti-inflammatory drugs, the interaction between LPS and host defense peptides has been previously investigated in literature. For example, Andrä et al. reported on LPS interactions with the peptide NK-2, demonstrating both hydrophobic and electrostatic interactions to be necessary for efficient LPS neutralization (33). Addressing the issue of binding localization and preference, Yang et al., found the rALF-Pm3 peptide to bind to a similar extent to lipid A and LPS, but with a higher affinity to lipid A (34). Similarly, Brandenburg et al. demonstrated preferential binding of lactoferrin to lipid A (35). These findings are in line with the present findings for GKS26, demonstrating a comparable adsorption density at LPS and its lipid A moiety, despite considerably less binding sites in the latter. Also addressing the issue of binding affinity, Singh et al. investigated the binding of cationic peptides is stronger for LPS than for the lipid membrane, and strongest for the lipid A moiety of LPS (27). Thus, the presence of both membrane-bound and non-adsorbed LPS will compete successfully with the liposomes for peptide and prevent its incorporation and disruption of the liposome membranes, in agreement with the present finding of substantially reduced liposome leakage induction by GKS26 in the presence of LPS. While there may certainly be a barrier function of LPS contributing to this effect as well (20), results on antimicrobial effects for Gram-negative bacteria show that this barrier function is not sufficient for preventing the fraction of peptides not bound to LPS to incorporate into the bacteria membrane and disrupt these. Also in line with findings of the present investigation,

conformational transitions in peptide/LPS complexes has previously been correlated to anti-inflammatory effects, e.g., for fowlicidin-1 fragments (36). In this context, it is worth noting that peptide-induced LPS packing transitions, may also contribute to peptide anti-endotoxic effects. For example, both are likely to facilitate phagocytosis, in analogy to size and charge dependence of phagocytosis of other types of nanoparticular systems (37). Through this, an alternative pathway to inflammation-triggering LPS-LBP/CD14 binding/activation is provided. Indeed, such phagocytosis-based anti-inflammatory scavenging has been previously observed for inflammation caused by amyloid Aβ (38).

Given LPS-induced exposure of both helix A and D on HCII activation, it interesting to compare the findings of the present investigation of helix A-derived GKS26 with those obtained for the analogous helix D-derived KYE28 (KYEITTIHNLFRKLTHRLFRRNFGYTLR). As GKS26, KYE28 was previously found to be antimicrobial against both Gram-negative and Gram-positive bacteria. Analysis of peptide effects on liposomes and supported lipid bilayers showed that antibacterial action by KYE28 is caused by direct membrane rupture, where the peptide binds at high density to the lipid membrane, insert into this without insertion threshold, and destabilize the membrane (27). In addition, like GKS26, KYE28 binds extensively to both LPS and its lipid A moiety, inducing pronounced helix formation in the peptide/LPS complex. Liposome leakage experiments in the presence and absence of LPS furthermore showed KYE28 to bind preferentially to LPS over the lipid membrane, again in agreement with the present results for GKS26. Also from a biological effect perspective, GKS26 and KYE28 behave similarly, as both effectively arrobogate adverse LPS effects.

Although the biological significance of the latter effects remains to be clarified, the potent antimicrobial and anti-inflammatory effects of GKS26, as well as limited toxicity and restoring effects on platelets, coagulation, and overall status, indicates a therapeutic potential of this peptide, offering likely advantages compared to the HCII holoprotein related to a lower cost of goods and increased stability. As with most macromolecular therapeutics, peptides of this size will most likely have to be administred parenterally. With its positive charge and intermediate hydrophobicity, even such routes may provide challenges in the form of serum protein binding and uptake in the reticuloendothelial system (RES), resulting in shortened bloodstream circulation time and reduced bioavailability. Various approaches can be employed for reducing such effects, including conjugation with poly(ethylene glycol) or incorporation of the peptide in a suitable drug carrier (39,40). In addition, for continuous infusion, the most likely administration of peptides against severe infection and sepsis, such serum protein scavenging does generally not affect bioavailability detrimentally as peptide is constantly replentished.

Conclusions

The peptide GKS26, derived from the A domain of HCII, displays potent antimicrobial effects, also at physiological salt concentration and in the presence of plasma and serum, related to peptide binding and destabilization of bacterial lipid membranes. In addition, GKS26 binds extensively to both LPS and its endotoxic moiety lipid A, and displays potent anti-inflammatory effects. The latter extend also to *in vivo* models of mice challenged with ip injection of LPS, where GKS26 suppresses pro-inflammatory cytokines, reduces vascular leakage and infiltration of inflammatory cells, and normalizes coagulation times. Given this, GKS26 may have therapeutic potential against severe infection and sepsis.

Acknowledgement

This work was supported by the Swedish Research Council (projects 2012-1842 and 2012-1883) and XImmune AB. Generous access to the DPI instrumentation from Biolin Farfield is gratefully acknowledged, as is valuable scientific discussion on the DPI results with Marcus Swann and Usha Devi at Biolin Farfield. Björn Walse is gratefully acknowledged for help with the HCII picture, and for valuable discussions. Finally, Lise-Britt Wahlberg and Ann-Charlotte Strömdahl are gratefully acknowledged for technical support.

References

1. Hancock, R.E. and Sahl, H.G. (2006) Antimicrobial and host-defense peptides as new anti-infective therapeutic strategies. *Nat. Biotechnol.* **24**, 1551-1557.
2. Elsbach, P. (2003) What is the real role of antimicrobial polypeptides that can mediate several other inflammatory responses? *J. Clin. Invest.* **111**, 1643-1645.
3. Pasupuleti, M., Schmidtchen, A., and Malmsten, M. (2012) Antimicrobial peptides: key components of the innate immune system. *Crit. Rev. Biotechnol.* **32**, 143-171.
4. Papareddy, P., Rydengård, V., Pasupuleti, M., Walse, B., Mörgelin, M., Chalupka, A., Malmsten, M., and Schmidtchen, A. (2011) Proteolysis of human thrombin generates novel host defense peptides. *PLoS Pathogens* **6**, e1000857, 1-15.
5. Kasetty, G., Papareddy, P., Kalle, M., Rydengård, V., Walse, B., Svensson, B., Mörgelin, M., Malmsten, M., and Schmidtchen, A. (2011) The C-terminal sequence of several human serin proteases encodes host defense functions. *J. Innate Immun.* **3**, 471-482.
6. Kalle, M., Papareddy, P., Kasetty, G., Tollefsen, D.M., Malmsten, M., Mörgelin, M., and Schmidtchen, A. (2013) Proteolytic activation transforms heparin cofactor II into a host defense molecule. *J. Immunol*. **190**, 6303-6310.
7. Kalle, M., Papareddy, P., Kasetty, G., Mörgelin, M., Van der Plas, M.J.A., Rydengård, V., Malmsten, M., Albiger, B., and Schmidtchen, A. (2012) Host defense peptides of thrombin modulate inflammation and coagulation in endotoxin-mediated shock and *P. aeruginosa* sepsis. *PLoS One* **7**, e51313, 1-11.
8. Strömstedt, A.A., Ringstad, L., Schmidtchen, A., and Malmsten, M. Interaction between amphiphilic peptides and phospholipid membranes. *Curr. Opinion Colloid Interface Sci*. **15** (2010) 467-478.

9. Malmsten, M. (1994) Ellipsometry studies of protein layers adsorbed at hydrophobic surfaces. *J. Colloid Interface Sci.* **166**, 333-342.

10. Malmsten, M., Burns, N., and Veide, A. (1998) Electrostatic and hydrophobic effects of oligopeptide insertions on protein adsorption. *J. Colloid Interface Sci.* **204**, 104-111.

11. Ringstad, L., Schmidtchen, A., and Malmsten, M. (2006) Effect of peptide length on the interaction between consensus peptides and DOPC/DOPA bilayers. *Langmuir* **22**, 5042-5050.

12. Mashagi, A., Swann, M., Popplewell, J., Textor, M., and Reimhult, E. (2008) Optical anisotropy of supported lipid structures probed by waveguide spectroscopy and its application to study of supported lipid bilayer formation kinetics. *Anal. Chem.* **80**, 3666-3676.

13. Yu, L., Guo, L., Ding, J.L., Ho, B., Feng, S.-S., Popplewell, J., Swann, M., and Wohland, T. (2009) Interaction of an artificial antimicrobial peptide with lipid membranes. *Biochim. Biophys. Acta* **1788**, 333-344.

14. Orädd, G., Schmidtchen, A., and Malmsten, M. (2011) Effects of peptide hydrophobicity on its incorporation in phospholipid membranes – an NMR and ellipsometry study. *Biochim. Biophys. Acta* **1808**, 244-252.

15. Lehrer, R. I., Rosenman, M., Harwig, S. S., Jackson, R., and Eisenhauer, P. (1991) Ultrasensitive assays for endogenous antimicrobial polypeptides, *J. Immunol. Methods* **137**, 167-173.

16. Andersson, E., Rydengard, V., Sonesson, A., Mörgelin, M., Bjorck, L., and Schmidtchen, A. (2004) Antimicrobial activities of heparin-binding peptides, *Eur. J. Biochem.* **271**, 1219-1226.

17. Pollock, J.S., Forstermann, U., Mitchell, J.A., Warner, T.D., Schmidt, H.H., Nakane, M., and Murad, F. (1991) Purification and characterization of particulate endothelium-derived relaxing factor synthase from cultured and native bovine aortic endothelial cells. *Proc. Natl. Acad. Sci. USA* **88**, 10480-10484.

18. Malmsten, M. (1994) Ellipsometry studies of protein adsorption at lipid surfaces. *J. Colloid Interface Sci.* **168**, 247-254.

19. Price, M.E., Cornelius, R.M., and Brash, J.L. (2001) Protein adsorption to polyethylene glycol modified liposomes from fibrinogen solution and from plasma. *Biochim. Biophys. Acta* **1512**, 191-205.

20. Schmidtchen, A. and Malmsten, M. (2013) Peptide interactions with bacterial lipopolysaccharides. *Curr. Opinion Colloid Interface Sci*. **18**, 381-392.

21. Wright, S.D., Ramos, R.A., Tobias, P.S., Ulevitch, R.J., and Mathison, J.C. (1990) CD14, a receptor for complexes of lipopolysaccharide (LPS) and LPS binding protein, *Science* **249**, 1431-1433.

22. Schumann, R.R., Leong, S.R., Flaggs, G.W., Gray, P.W., Wright, S.D., Mathison, J.C., Tobias, P.S., and Ulevitch, R.J. (1990) Structure and function of lipopolysaccharide binding protein. *Science* **249**, 1429-1431.

23. Shimazu, R., Akashi, S., Ogata, H., Nagai, Y., Fukudome, K., Miyake, K., and Kimoto, M. (1999) MD-2, a molecule that confers lipopolysaccharide responsiveness on toll-like receptor 4. *J. Exp. Med.* **189**, 1777-1782.

24. Esmon, C.T. The interactions between inflammation and coagulation. (2005) *Br. J. Haematol.* **131**, 417-430.

25. Mayeux, P.R. (1997) Pathobiology of lipopolysaccharide. *J. Toxicol. Environ. Health* **51**, 415-435.

26. Lee, T.-H., Heng, C., Swann, M.J., Gehman, J.D., Separovic, F., and M.-I. Aguilar (2010) Real-time quantitative analysis of lipid disordering by aurein 1.2 during membrane adsorption and lysis. *Biochim. Biophys. Acta* **1798**, 1977-1986.

27. Singh, S., Papareddy, P., Kalle, M., Schmidtchen, A., and Malmsten, M. (2013) Importance of lipopolysaccharide aggregate disruption for the anti-endotoxic effect of heparin cofactor II peptides. *Biochim. Biophys. Acta* **1828**, 2709-2719.

28. Singh, S., Kasetty, G., Schmidtchen, A., and Malmsten, M. (2012) Membrane and lipopolysaccharide interactions of C-terminal peptides from S1 peptidases. *Biochim. Biophys. Acta* **1818**, 2244-2251.

29. Schmidtchen, A., Ringstad, L., Kasetty, G., Mizuno, H., Rutland, M.W., and Malmsten, M. (2011) Membrane selectivity by W-tagging of antimicrobial peptides. *Biochim. Biophys. Acta* **1808**, 1081-1091.

30. Mueller, M., Lindner, B., Kusumoto, S., Fukase, K., Schromm, A.B., and Seydel, U. (2004) Aggregates are the biologically active units of endotoxin. *J. Biol. Chem.* **279**, 26307-26313.

31. Rosenfeld, Y., Papo, N., and Shai, Y. (2006) Endotoxin (lipopolysaccharide) neutralization by innate immunity host-defense peptides. *J. Biol. Chem.* **281**, 1636-1643.

32. Rosenfeld, Y., Sahl, H.-G., and Shai, Y. (2008) Parameters involved in antimicrobial and endotoxin detoxification activities of antimicrobial peptides. *Biochemistry* **47**, 6468-6478.

33. Andrä, J., Koch, M.H., Bartels, R., and Brandenburg, K. (2004) Biophysical characterization of endotoxin inactivation by NK-2, an antimicrobial peptide derived from mammalian NK-lysin. *Antimicrob. Agents Chemother*. **48**, 1593-1599.

34. Yang, Y., Boze, H., Chemardin, P., Padilla, A., Moulin, G., Tassanakajon, A., Pugniere, M., Roquet, F., Destoumieux-Garzon, D., Gueguen, Y., Bachere, E., and Aumelas, A. (2009) NMR structure of rALF-Pm3, an anti-lipopolysaccharide factor from shrimp: model of the possible lipid A-binding site. *Biopolymers* **91**, 207-220.

35. Brandenburg, K., Jürgens, G., Müller, M., Fukuoka, S., and Koch, M.H.J. (2001) Biophysical characterization of lipopolysaccharide and lipid A inactivation by lactoferrin, *Biol. Chem*. **382**, 1215-1225.

36. Bhunia, A., Mohanram, H., and Bhattacharjya, S. (2009) Lipopolysaccharide bound structures of the active fragments of fowlicidin-1, a cathelicidin family of antimicrobial and antiendotoxic peptide from chicken, determined by transferred nuclear Overhauser effect spectroscopy. *Peptide Science* **92**, 9-22.

37. Sahay, G., Alakhova, D.Y., and Kabanov, A.V. (2010) Endocytosis of nanomedicines. *J. Controlled Release* **145**, 182-195.

38. Richman, M., Perelman, A., Gertler, A., and Rahimipour, S. (2013) Effective targeting of Aβ to macrophages by sonochemically prepared surface-modified protein microspheres. *Biomacromolecules* **14**, 110-116.

39. Veronese, F.M. and Mero, A. (2008) The impact of PEGylation on biological therapies. *Biodrugs* **22**, 315-329.

40. Bysell, H., Månsson, R., Hansson, P., and Malmsten, M. (2011) Microgels and microcapsules in peptide and protein delivery. *Adv. Drug Delivery Rev*. **63**, 1172-1185.

41. Kyte, J., and Doolittle, R.F. (1982) A simple method for displaying the hydropathic character of a protein. *J. Mol. Biol.* **157**, 105-132.

Table 1. Sequence and key properties of GKS26.

	Sequence	*IP*[1]	Z_{net}[2] *(pH 7.4)*	*H*
GKS26	GKSRIQRLNILNAKFAFNLYRVLKDQ	11.49	+5	-0.42

[1] IP:isoelectric point; [2]Z_{net}: net charge; [3]H mean hydrophobicity on the Kyte-Doolittle scale (41).

Figure Captions

Figure 1. Antimicrobial activity. (**A**) Antimicrobial activity of GKS26 (at 100 µM), as obtained by RDA, against the indicated microbes. Bacteria (4 x 10^6 cfu) were inoculated in 0.1% TSB agarose gel, followed by peptide addition to 4 mm-diameter wells. Clearance zones correspond to the inhibitory effect of each peptide after incubation at 37 °C for 18-24 h. (**B**) Antibacterial effects of GKS26 against the indicated bacterial strains in viable count assays. 2 x 10^6 cfu/ml bacteria were incubated in 50 µl with peptides at the indicated concentrations in 10 mM Tris, containing 0.15 M NaCl (buffer), in 10 mM Tris, 0.15 M NaCl, pH 7.4, containing 20% human citrate plasma (CP), or in 20% human serum (Serum). (**C**) Kinetics of GKS26 killing of *E. coli* and *P. aeruginosa* at a peptide concentration of 3 µM in 10 mM Tris, 0.15 M NaCl, pH 7.4. (n=3)

Figure 2. GKS26 toxicity vs antimicrobial activity in human whole blood. The indicated bacteria (2 x 10^8 cfu/ml) were incubated in 50% human citrate blood with or without 60 and 120 µM of peptide, followed by determination of cfu by VCA (**A**) and hemolysis (**B**). (n=3)

Figure 3. Permeabilizing effects of GKS26 on bacteria. (**A**) *E. coli* was incubated with 30 µM peptide in 10 mM Tris, pH 7.4, and permeabilization assessed using the impermeant probe FITC. (**B**) Scanning electron microscopy images of *P. aeruginosa* and *S. aureus* before and after incubation with 30 µM peptide for 2 h at 37 °C.

Figure 4. Liposome leakage induction. Peptide-induced liposome leakage for *E. coli* and DOPE/DOPG (75/25 mol/mol) liposomes, as well as leakage from DOPE/DOPG liposomes in the presence of 0.02 mg/ml *E. coli* LPS. Measurements were performed in 10 mM Tris, pH 7.4. (n=3)

Figure 5. Peptide adsorption. (**A**) Peptide binding to supported DOPE/DOPG (75/25 mol/mol) bilayers. (**B**) Peptide-induced membrane destabilization, monitored by DPI for DOPE/DOPG supported bilayers (75/25 mol/mol). Measurements were performed in 10 mM Tris, pH 7.4, and data reported as reduction in Δn_f, the lipid membrane birefringence, (due to peptide insertion and membrane disordering) as a function of the adsorption density of the peptide. (**C**) CD spectra in 10 mM Tris, pH 7.4, the absence and presence of DOPE/DOPG liposomes (75/25 mol/mol; 100 μM lipid). (n=3).

Figure 6. (**A**) Peptide binding to *E. coli* LPS and *E. coli* lipid A. (**B**) CD spectra for GKS26 with or without *E. coli* LPS (0.2 mg/ml). Shown also is the CD spectrum for LPS in the absence of peptide. Measurements were performed in 10 mM Tris, pH 7.4. (n=3).

Figure 7. Effects of GKS26 on LPS-induced responses *in vitro*. (**A**) RAW 264.7 macrophages were stimulated with 10 ng/ml *E. coli* LPS in combination with indicated concentrations of GKS26. Nitric oxide production was determined in the cell supernatants using the Griess reaction (n=3, mean±SEM). (**B**) RAW Blue cells were stimulated with indicated concentrations of *E. coli* LPS and 10 μM of GKS26. NF-κB activation was measured after 20 h (n=5). (**C**) LDH release in supernatants of RAW-Blue cells from the experiments in (**B**) (n=3). (**D**) Human lepirudin-treated blood was stimulated with 100 ng/ml *E. coli* LPS in combination with 10 μM GKS26. Indicated cytokines were measured in plasma after 20 h of incubation (n=5).

Figure 8. Effects of GKS26 on LPS-induced responses *in vivo*. Septic shock in C57BL/6 mice was induced by intraperitoneal (ip) injection of *E. coli* LPS (18 mg/kg) followed by ip

injection of 200 or 500 μg of GKS26 or buffer. Effects were assessed 20 h post LPS-challenge. (**A**) Indicated cytokines were analysed in plasma (LPS n=12, $GKS26_{200\mu g}$ n= 5, $GKS26_{500\mu g}$ n=11). (**B**) Scoring of mice status 20 hours after LPS injection. (1; healthy, 4; septic shock (most severe scoring); Control n= 6, LPS n=12, $GKS26_{200\mu g}$ n= 6, $GKS26_{500\mu g}$ n=11). (**C**) Activated partial thromboplastin time (aPTT) and prothrombin time (PT) were measured using citrate plasma (Control n= 6, LPS n=10, $GKS26_{200\mu g}$ n= 5, $GKS26_{500\mu g}$ n=11; Median indicated). (**D**) Number of platelets was determined in mice 20 hours after injection of LPS and treatment with GKS26 (Control n= 6, LPS n=12, $GKS26_{200\mu g}$ n= 5, $GKS26_{500\mu g}$ n=11). (**E**) Lungs of non-treated (Control), LPS-challenged, and GKS26-treated mice were analyzed by histology. Representative light microscopy images stained with haematoxylin-eosin (magnification 4x) are shown.

Figure 1.

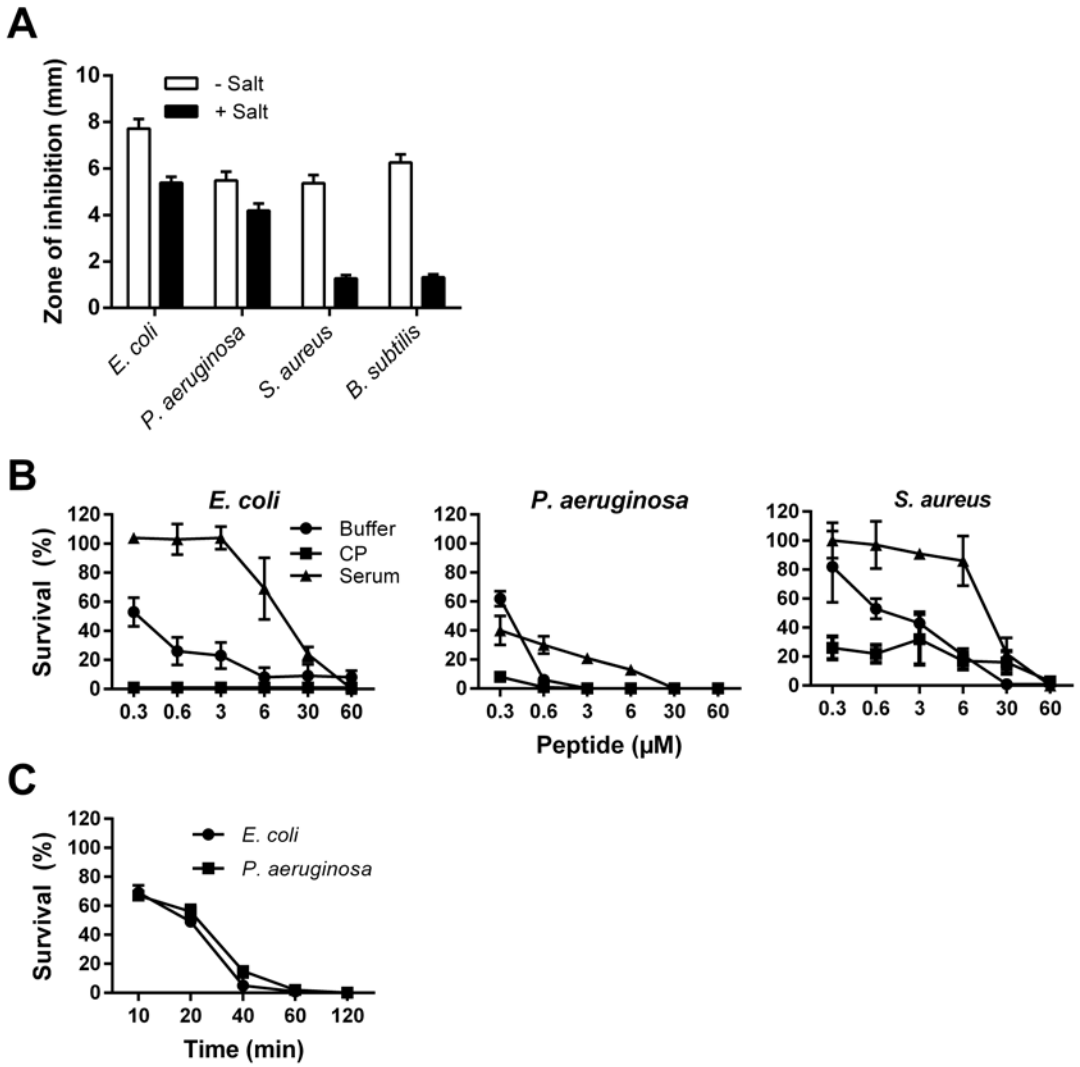
A
Zone of inhibition (mm)
- Salt
+ Salt
E. coli
P. aeruginosa
S. aureus
B. subtilis
B
E. coli
P. aeruginosa
S. aureus
Survival (%)
Buffer
CP
Serum
Peptide (μM)
C
E. coli
P. aeruginosa
Survival (%)
Time (min)

Figure 2.

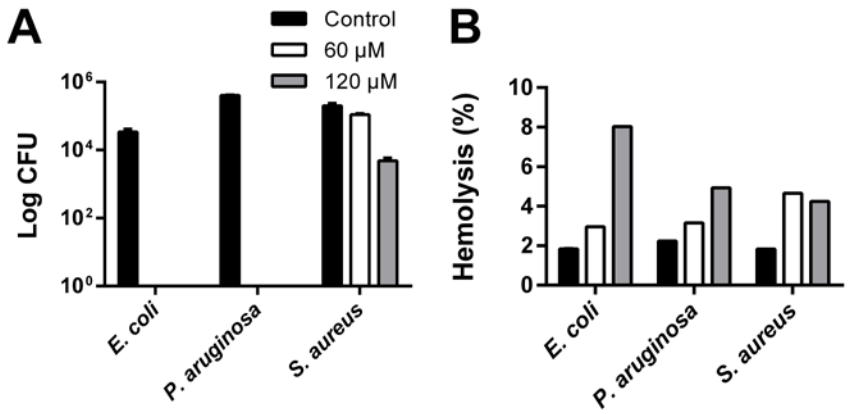
A
Control
60 μM
120 μM
Log CFU
10^6
10^4
10^2
10^0
E. coli
P. aruginosa
S. aureus
B
Hemolysis (%)
10
8
6
4
2
0
E. coli
P. aruginosa
S. aureus

Figure 3.

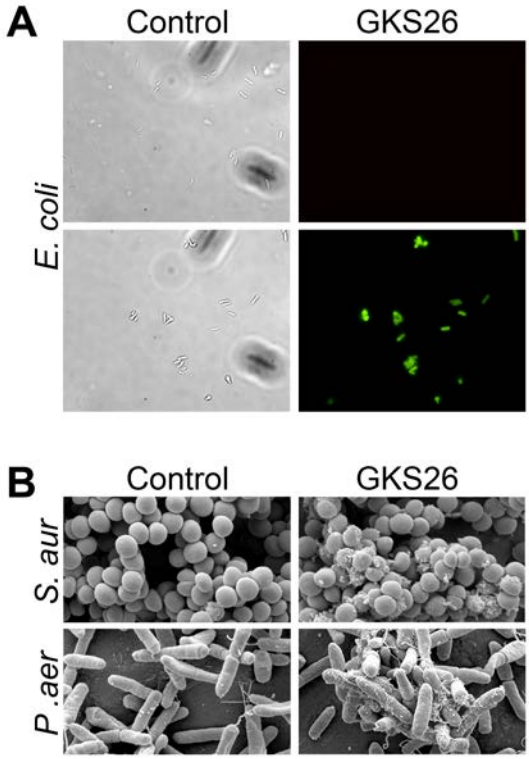

Figure 4.

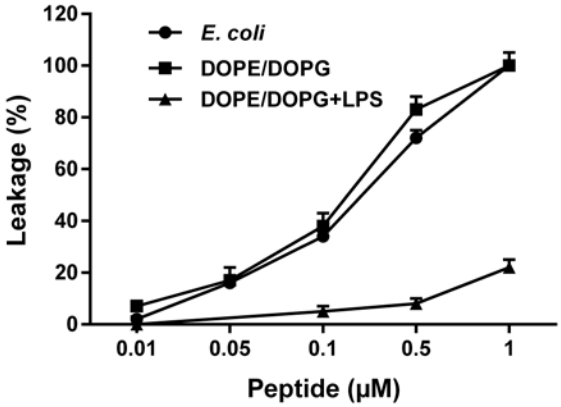
E. coli
DOPE/DOPG
DOPE/DOPG+LPS
Leakage (%)
120
100
80
60
40
20
0
0.01
0.05
0.1
0.5
1
Peptide (μM)

Figure 5.

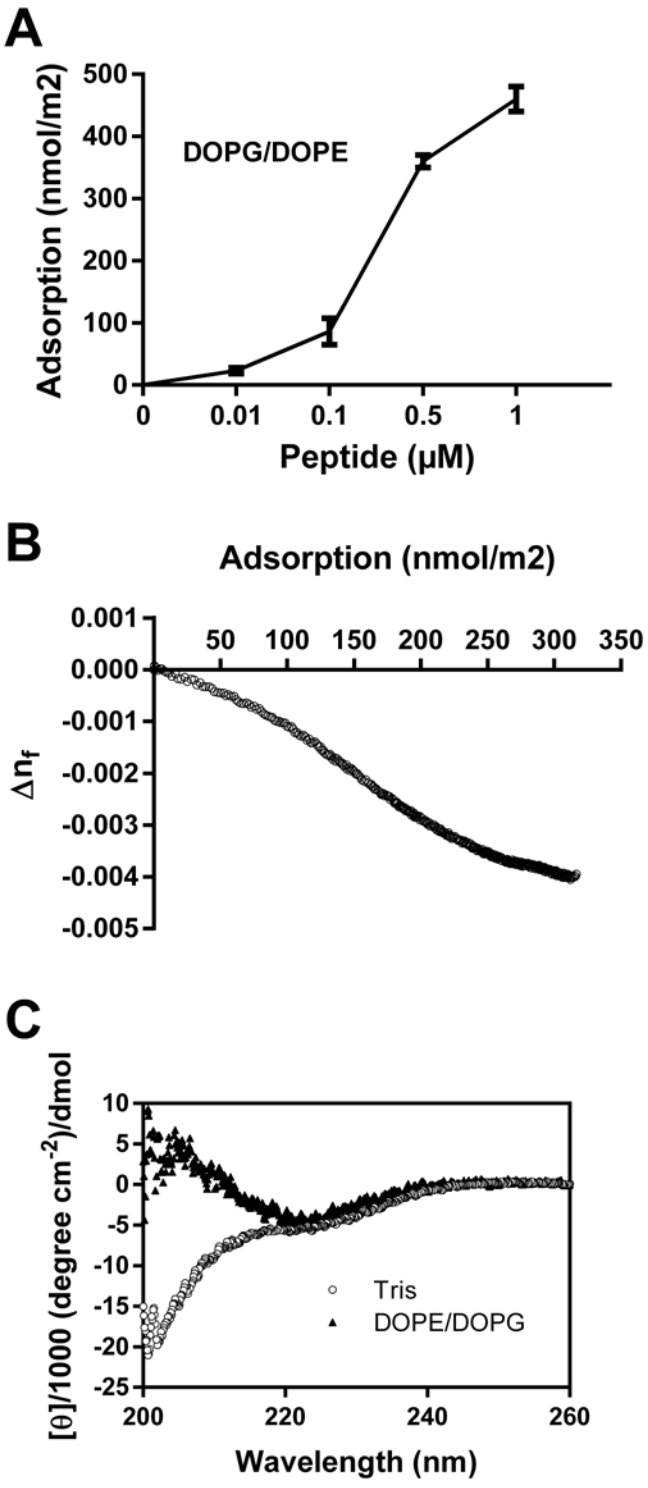
A
Adsorption (nmol/m2)
500
400
300
200
100
0
DOPG/DOPE
0
0.01
0.1
0.5
1
Peptide (μM)
B
Adsorption (nmol/m2)
0.001
0.000
-0.001
-0.002
-0.003
-0.004
-0.005
Δnf
50
100
150
200
250
300
350
C
[θ]/1000 (degree cm-2)/dmol
10
5
0
-5
-10
-15
-20
-25
Tris
DOPE/DOPG
200
220
240
260
Wavelength (nm)

Figure 6.

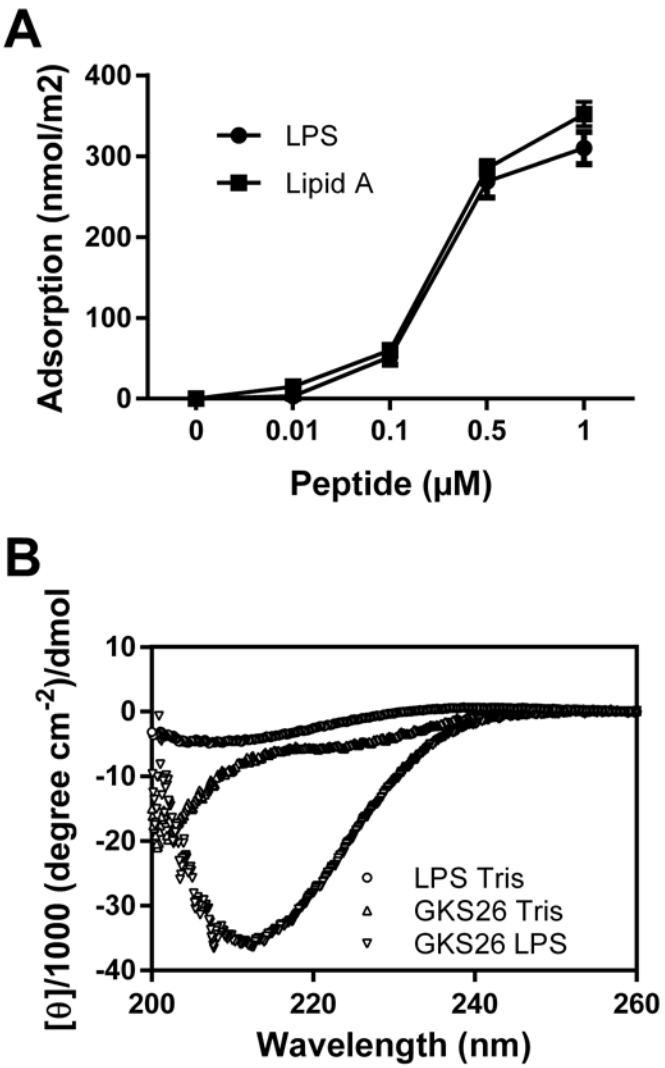
A
Adsorption (nmol/m2)
400
300
200
100
0
LPS
Lipid A
0
0.01
0.1
0.5
1
Peptide (μM)
B
[θ]/1000 (degree cm-2)/dmol
10
0
-10
-20
-30
-40
LPS Tris
GKS26 Tris
GKS26 LPS
200
220
240
260
Wavelength (nm)

Figure 7.

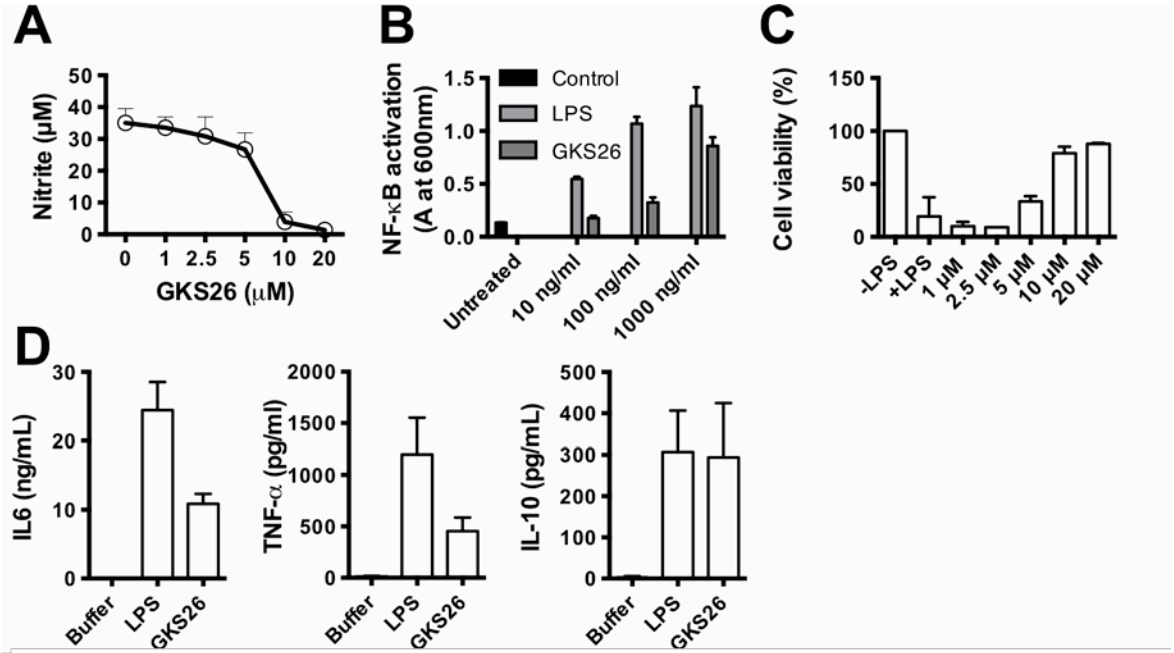
A
Nitrite (μM)
50
40
30
20
10
0
0 1 2.5 5 10 20
GKS26 (μM)
B
NF-κB activation (A at 600nm)
1.5
1.0
0.5
0.0
Control
LPS
GKS26
Untreated
10 ng/ml
100 ng/ml
1000 ng/ml
C
Cell viability (%)
150
100
50
0
-LPS
+LPS
1 μM
2.5 μM
5 μM
10 μM
20 μM
D
IL6 (ng/mL)
30
20
10
0
Buffer
LPS
GKS26
TNF-α (pg/ml)
2000
1500
1000
500
0
Buffer
LPS
GKS26
IL-10 (pg/mL)
500
400
300
200
100
0
Buffer
LPS
GKS26

Figure 8.

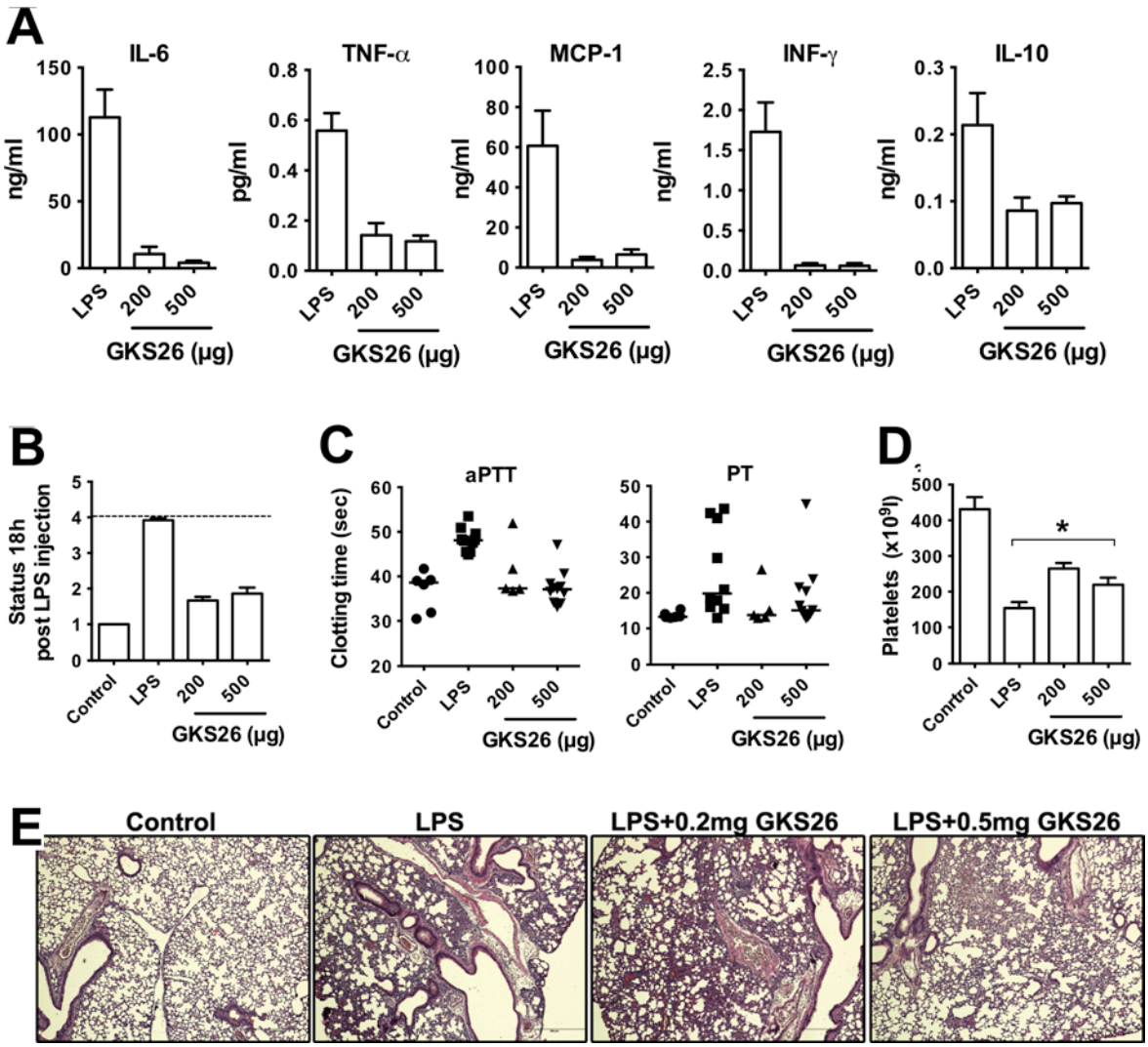
A
IL-6
ng/ml
150
100
50
0
LPS
200
500
GKS26 (μg)
TNF-α
pg/ml
0.8
0.6
0.4
0.2
0.0
MCP-1
ng/ml
100
80
60
40
20
0
INF-γ
ng/ml
2.5
2.0
1.5
1.0
0.5
0.0
IL-10
ng/ml
0.3
0.2
0.1
0.0
B
Status 18h post LPS injection
5
4
3
2
1
0
Control
LPS
200
500
GKS26 (μg)
C
aPTT
Clotting time (sec)
60
50
40
30
20
PT
50
40
30
20
10
0
Control
LPS
200
500
GKS26 (μg)
D
Platelets (x10⁹/l)
500
400
300
200
100
0
*
Conrtrol
LPS
200
500
GKS26 (μg)
E
Control
LPS
LPS+0.2mg GKS26
LPS+0.5mg GKS26